Airey, G.D. and Collop, A.C. (2014) Mechanical and structural assessment of laboratory- and field-compacted asphalt mixtures. International Journal of Pavement Engineering, 17 (1). pp. 50-63. ISSN 1477-268X

International Journal of Pavement Engineering

ISSN: 1029-8436 (Print) 1477-268X (Online) Journal homepage: http://www.tandfonline.com/loi/gpav20

Mechanical and structural assessment of laboratory- and field-compacted asphalt mixtures

G.D. Airey & A.C. Collop

To cite this article: G.D. Airey & A.C. Collop (2016) Mechanical and structural assessment of laboratory- and field-compacted asphalt mixtures, International Journal of Pavement Engineering, 17:1, 50-63, DOI: 10.1080/10298436.2014.925551

To link to this article: http://dx.doi.org/10.1080/10298436.2014.925551

Published online: 16 Jun 2014.

International Journal of Pavement Engineering, 2015
Vol. 17, No. 1, 50–63, http://dx.doi.org/10.1080/10298436.2014.925551

Mechanical and structural assessment of laboratory- and field-compacted asphalt mixtures

G.D. Airey* and A.C. Collop

Nottingham Transportation Engineering Centre, University of Nottingham, Nottingham NG7 2RD, UK

(*Received 21 May 2013; accepted 22 June 2013*)

Compaction forms an integral part in the formation of the aggregate orientation and structure of an asphalt mixture and therefore has a profound influence on its final volumetric and mechanical performance. This article describes the influence of various forms of laboratory (gyratory, vibratory and slab-roller) and field compaction on the internal structure of asphalt specimens and subsequently on their mechanical properties, particularly stiffness and permanent deformation. A 2D image capturing and image analysis system has been used together with alternative specimen sizes and orientations to quantify the internal aggregate structure (orientation and segregation) for a range of typically used continuously graded asphalt mixtures. The results show that in terms of aggregate orientation, slab-compacted specimens tend to mimic field compaction better than gyratory and vibratory compaction. The mechanical properties of slab-compacted specimens also tend to be closer to that of field cores. However, the results also show that through careful selection of specimen size, specimen orientation and compaction variables, even mould-based compaction methods can be utilised with particular asphalt mixtures to represent field-compacted asphalt mixtures.

Keywords: compaction; asphalt mixtures; gyratory; slab; image analysis; aggregate skeleton; stiffness modulus; permanent deformation

Introduction

High-quality asphalt mixture compaction is an essential factor in the design and subsequent production of high-quality pavements. Achieving consistency in compaction, both in the laboratory and in the field, is necessary if accurate correlation is to occur between laboratory performance and observed field behaviour. Laboratory compaction provides a more controlled environment (smaller material quantities, tighter temperature and compaction energy controls, etc) than that found for field compaction. However, experience has shown that, first, different modes of laboratory compaction tend to produce asphalt mixtures with significantly different mechanical properties and, second, that these mechanical properties can differ considerably from those obtained from field specimens.

The fact that different modes of compaction create volumetrically identical but mechanically different specimens has long been recognised (Vallerga 1951, Nevitt 1959). In recent years, various studies have been undertaken to assess the influence of both laboratory and field compaction on the mechanical performance of the asphalt mixture (Consuegra *et al.* 1989, Sousa *et al.* 1991, Von Quintas *et al.* 1991, Harvey and Monismith 1993, Brown and Gibb 1999, Renken 2000, Hunter *et al.* 2004b, Airey *et al.* 2006). In addition, increased use has been made of image analysis techniques to study the internal aggregate arrangement of asphalt structures. These techniques consist of either non-destructive, X-ray computed tomography (X-ray CT) (Masad *et al.* 1999, Tashman *et al.* 2002) or 2D imaging using destructive (sawing) techniques combined with digital cameras (Yue *et al.* 1995, Shashidar 1999, Hunter *et al.* 2004a, Masad and Button 2004, Airey *et al.* 2006). It is generally accepted that differences in particle orientation and general aggregate structure caused by different compaction methods led to differences in mechanical performance with mould-based compaction methods (gyratory and vibratory) generally differing from roller-compacted slab specimens and field-compacted cores of comparable air voids.

This article considers the influence of laboratory compaction methods on the internal structure (aggregate orientation and segregation) as well as the mechanical properties (stiffness modulus, permanent deformation and fatigue) of the asphalt mixture relative to what is found for standard field compaction. To check the sensitivity of any findings to mixture type, a total of four asphalt mixtures were included in the study ranging from 14 mm maximum stone size surfacing material to 32 mm high modulus base (HMB) material. Three methods of laboratory compaction have been considered in this study: gyratory, vibratory and slab 'roller' compaction. These represent the most commonly used laboratory compaction methods in the UK. The compaction parameters were closely controlled and all the specimens were manufactured using the same constituent materials and mixture design procedure. The article also investigates the changes in aggregate

*Corresponding author. Email: gordon.airey@nottingham.ac.uk

orientation and mechanical performance for smaller specimens cored from larger specimens and, therefore, less affected by mould-confining effects associated with gyratory and vibratory compaction.

Materials and mixture design

The experimental testing programme included a wide range of asphalt mixtures as detailed in Table 1. The mixtures were carefully chosen to represent four nominal maximum aggregate sizes and a range of bituminous binders. In general, the larger the nominal maximum aggregate size, the greater the risk of segregation and non-uniform compaction.

The modes of laboratory compaction were chosen to represent those commonly used in the UK. Where possible the number of specimens tested for each compaction method and mixture was limited to 30 to provide a reasonable number for statistical analysis whilst being practical in terms of laboratory time. The sites that provided the field cores were made of the same constituent materials as those used in the laboratory testing programme.

Compaction methods

The mixing and compaction temperatures were carefully controlled for all compaction modes to ensure high-quality compaction and appropriate bitumen viscosities in line with the relevant standards (BS EN 12697-31, 32, 33 & 35). After mixing, the loose asphalt mixture was poured onto a tray and mixed manually using the 'cone and quarter' method in an effort to reduce segregation. The opposing diagonal quarters of the mixture were then added to the moulds ready for compaction. Care was taken to ensure that the mixture did not drop below the temperature of 150°C. Once the specimens had been manufactured they were cut using a diamond-edged circular saw.

Gyratory compaction

Two types of gyratory compactors were used in the study consisting of a 'Cooper Research Technology' compactor manufactured in the UK and the French 'Laboratoire Central des Ponts et Chaussees (LCPC)' gyratory compactor. The gyratory compaction parameters used with the Cooper compactor complied with BS EN 12697-31 and consisted of a compaction pressure of 600 kPa, a gyratory angle of 1.25° and a gyration rate of 30 gyrations per minute. The parameters used with the LCPC gyratory compactor consisted of a slightly higher compaction pressure of 662 kPa and a lower angle of 55′ with the same rate of 30 gyrations per minute.

The specimens were all compacted to a target density, as opposed to a set number of gyrations, although the number of gyrations never exceeded 300 gyrations (10 minutes). The 28-mm dense bitumen macadam (DBM), 14-mm surfacing and 32-mm HMB asphalt mixtures were compacted in 150-mm diameter moulds, whereas the 20-mm HMB asphalt mixture was compacted in 100-mm diameter moulds. During the compaction programme, silicon spray was used on the inside of the moulds to ease subsequent specimen extraction.

Vibratory compaction

An electric vibratory hammer was used to compact the specimens in a split mould of internal diameter 152.45 ± 0.5 mm according to BS EN 12697-32. The power consumption of the vibratory hammer was 800 W

Table 1. Asphalt mixtures included in the testing programme.

	Percentage passing			
Aggregate gradation sieve sizes	28-mm DBM	20-mm HMB	14-mm DBM	32-mm HMB
37.5 mm	100			100
28 mm	98	100		89
20 mm	83	98	100	83
14 mm	68	77	98	70
10 mm		62	80	
6.3 mm	52	47	60	53
3.35 mm	38	40	43	39
0.3 mm	14	14	16	15
0.075 mm	7	7	9	8
Aggregate	Limestone	Limestone	Granite	Limestone
Bitumen	40/60 pen	30/45 pen	SBS PMB[a]	30/45 pen
Binder content (%)	4	4.2	4.9	4
Maximum density (kg/m^3)	2513	2465	2660	2482
Target void content (%)	4.2	3.6	3.6	4.2

[a] Class 4 for both penetration at 25°C and softening point according to EN 14023.

and operated at a frequency of 35 Hz. Consistently achieving a designated air voids using vibratory compaction is difficult and as a result there was some variance in the air void content of these specimens.

Steel slab roller compaction

The steel slab roller compactor consisted of a curved steel segment, pivoting on a hinge and applying the load via pneumatic actuators. The asphalt mixture was placed in a steel mould (internal dimensions of 300 mm by 300 mm by 140 mm) which moved back and forth beneath the roller. The partial free face allowed the aggregates to orient themselves in a manner similar to that which occurs on site (Consuegra *et al.* 1989). The precise depth of the compacted asphalt layer was set at the start of the test based on the knowledge of the maximum density of the mixture and mass of the slab to enable a target air void content to be specified. The direct force applied to the slab was not measured, but complied with BS EN 12697-33, which specifies a minimum static load, F, that the device should apply:

$$\frac{F}{2Dl} \geq 10^{-5}, \quad (1)$$

where F is the load applied onto the roller (kN), l is the interior width of the mould (mm) and D is the diameter of the wheel or roller (mm). The dimensions of resulting slabs were 300 mm × 300 mm × 100 mm. This enabled two 150-mm diameter specimens or four 100-mm diameter specimens to be cored from each slab. The specimen orientation for all roller-compacted specimens was perpendicular to the compaction force of the roller.

Field compaction

For the 28-mm DBM, 20-mm and 32-mm HMB, the initial compaction was carried out by a dead weight 12/14-t three-wheeled roller. Secondary compaction was undertaken by a Bomag 161, with a vibration-affected weight of 24t. The asphalt laying temperature was around 150°C for the 20-mm and 32-mm HMB and 140°C for the 28-mm DBM, with an air temperature of around 8°C. For the 14-mm asphalt mixture, the initial compaction was undertaken by a 12-t static dual roller HAMM compactor. Secondary compaction was undertaken by a Bomag 120 2.5-t tandem vibratory roller. The laying temperature was around 145°C with an air temperature of 13°C. The specimen orientation for all field-compacted specimens was perpendicular to the compaction force applied in the field.

Asphalt mixture mechanical properties

Stiffness modulus

The stiffness moduli of the asphalt mixture specimens were measured using the indirect tensile stiffness modulus (ITSM) test. The test is non-destructive and involves the application of load pulses to the vertical diameter of a cylindrical specimen, with the resultant peak transient deformation measured along the horizontal diameter. The stiffness modulus is then a function of load, deformation, specimen dimensions and an assumed Poisson's ratio of 0.35. The ITSM test was undertaken in accordance with recognised guidelines (BSI 1993) using the following test parameters:

Test temperature:	20°C
Loading rise-time:	124 milliseconds
Peak transient horizontal deformation:	7 μm (150-mm diameter specimen) 5 μm (100-mm diameter specimen)

The test specimen is initially conditioned through the application of five load pulses. A further five load pulses are then applied from which a mean stiffness modulus is obtained. The sample is then rotated through 90° and a further five pulses are applied and a resulting mean stiffness modulus obtained. The stiffness modulus of the asphalt mixture specimen is then calculated as the average of these two mean values.

Permanent deformation

The resistance of the asphalt mixture specimens to permanent deformation was determined by means of the repeated load axial test (RLAT) using a direct uniaxial compression testing configuration. The test consists of applying a number of load pulses to the flat faces of the specimen and recording the resulting deformation. The axial strain obtained at the end of the test is used as a measure of the specimen's resistance to permanent deformation. The RLAT was undertaken in accordance with recognised guidelines (BSI 1996) and the following test parameters:

Test temperature:	40°C
Test duration:	7200 s (3600 cycles)
Loading pattern:	1 s loading followed by a 1 s recovery period per cycle
Axial stress:	100 kPa
Conditioning stress:	10 kPa for 120 s

The permanent deformation performance of the asphalt mixtures was quantified by means of the ultimate percentage strain after 3600 cycles, although the rate of strain (microstrain per cycle) over the linear phase of the deformation response can also be used (Brown and Gibb 1996).

Fatigue cracking

The fatigue life of the asphalt mixture specimens was assessed using the indirect tensile fatigue test (ITFT) with

an experimental arrangement similar to that used for the ITSM test but under repeated loading conditions. A range of stress levels were chosen, and the number of pulses to failure (defined as the point at which there is 9 mm of vertical deformation) was recorded. The range of stress levels should ensure a wide range in fatigue lives with the test being carried out using the following test parameters (BSI 1995):

Test temperature:	20°C
Loading condition::	Controlled-stress
Rise time:	124 milliseconds
Pulse repetition:	1.5 ± 0.1 s (40 pulses/minute)
Range of tensile stress:	200–700 kPa

The maximum tensile strain generated at the centre of the specimen is defined as:

$$\varepsilon_{\text{xmax}} = \frac{\sigma_{\text{xmax}}(1+3\upsilon)}{S_{\text{m}}} \times 1000, \quad (2)$$

where $\varepsilon_{\text{xmax}}$ is the maximum tensile horizontal strain at the centre of the specimen in microstrain, σ_{xmax} is the maximum tensile stress at the centre of the specimen in kPa, υ is Poisson's ratio (assumed to be 0.35) and S_{m} is the indirect tensile stiffness modulus at σ_{xmax} in MPa. The maximum tensile stress at the centre of the specimen is defined as:

$$\sigma_{\text{xmax}} = \frac{2L}{\pi \text{d} t}, \quad (3)$$

where d is the diameter of the test specimen (m) and L is the vertical applied line load in kN. Linear regression analysis of the ITFT results was used to determine fatigue functions for the asphalt mixtures using the following relationship:

$$N_{\text{f}} = a\varepsilon_0^{-b}, \quad (4)$$

where N_{f} is fatigue life, ε_0 is the initial tensile strain (microstrain) and a, b are experimentally determined coefficients.

Aggregate skeleton matrix

Image analysis techniques

There are currently two main image analysis techniques available for the study of asphalt structures: (i) X-ray CT and (ii) digital cameras. X-ray CT is a completely non-destructive method for visualising features in the interior of solid objects to obtain digital information on their three-dimensional geometry and properties (Tashman *et al.* 2002). It operates by X-raying a series of planes within the specimen. The resulting intensity values are then correlated to the densities of the materials. The technique works well with a composite material such as asphalt as its three phases (air, bitumen and aggregate) have distinct densities. The computer software subsequently assimilates the information to produce a 2D or 3D digital image.

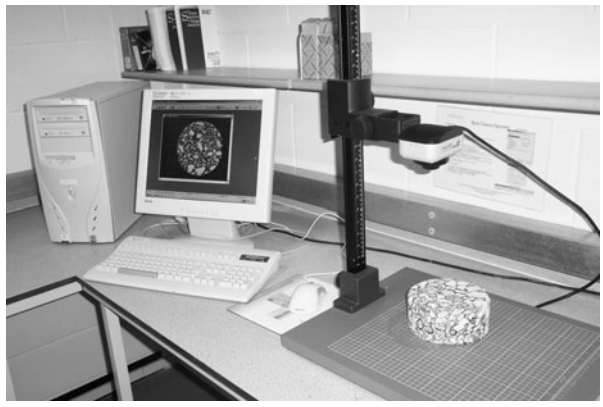

Figure 1. 2D image analysis equipment.

This study used a digital camera (QImaging Evolution MP 12 bit digital camera) and Image ProPlus software as shown in Figure 1. This is a destructive technique due to the need for cut sample surfaces and fails to capture the air void distribution but it has the advantage of capturing greater aggregate detail on an individual plane and being relatively inexpensive. The cores were cut using diamond-tipped saw blades and the surfaces marked, as shown in Figure 2. In total, 1200 monochrome images per compaction method and asphalt mixture type were taken with approximately 3000 aggregate particles captured on each slice.

A process called 'thresholding' was undertaken on the images to provide information on the contrast of different objects in the image. Image analysis is most effective where the objects of interest have distinct colour/lightness phases when compared to their surroundings. This is indicated in the threshold plot displayed in Figure 3. Plot A is representative of an image where the phases are readily distinguishable, whereas plot B is representative of an image where the phases are intertwined and hence difficult for any subsequent analysis. In this type of image analysis,

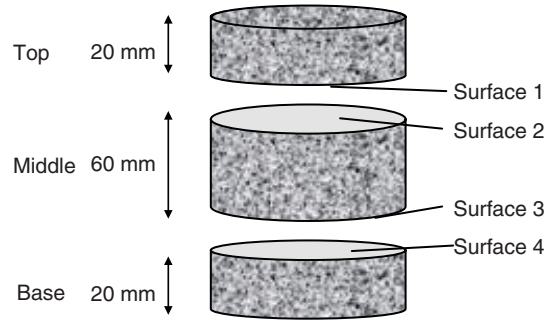

Figure 2. Core sections and surfaces of cylindrical specimens.

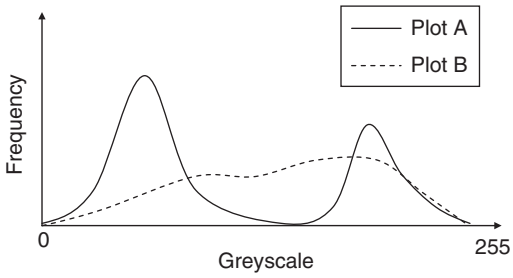

Figure 3. Schematic threshold intensity plots.

the monochrome contrast between the two materials, bitumen and aggregate, is critical to the success of the results. The image analysis software enables the user to automatically select light-coloured objects. In this instance, the software uses an algorithm based on the threshold data to make a judgement of what constitutes a light-coloured object, or in this instance the aggregate particles. Once the thresholding process has been undertaken, the user may perform a number of 'count and measure' operations on the objects selected. Virtually any measurement of a recognised particle can be made, for example area, particle orientation, centre of area, perimeter (Hunter *et al.* 2004a). In this study, the following parameters were measured:

- Visible particle cross-sectional area (VSA).
- The vertical particle angle (β), defined as the angle between the major axis length of the particle and the vertical axis. The vertical axis is provided by the image boundary.
- Centre of VSA (x_c, y_c) of the particle.
- The maximum length of the particle.
- The maximum width of the particle.

It should be noted that an element of the fines within the aggregate matrix are not recognised by the image analysis thresholding process, due to their size and the cutting process. The cutting process can discolour very small particles by smearing the adjacent bitumen over the area, hence reducing the contrast between the particle and the bitumen. With the knowledge of the mixture design and relative material densities, it is possible to calculate that the average aggregate surface area should be approximately 88% of the total area. Approximately 25% of the aggregate surface area was not recognised by the image analysis process. This 'aggregate loss' is not seen as a major problem in this study which is concerned with the structural effect of the aggregate generally provided by the larger particles as opposed to the bitumen mastic (filler-fines). Based on the parameters determined using the 2D system, the aggregate orientation (alignment) and segregation for the various asphalt mixtures as a function of compaction method were determined.

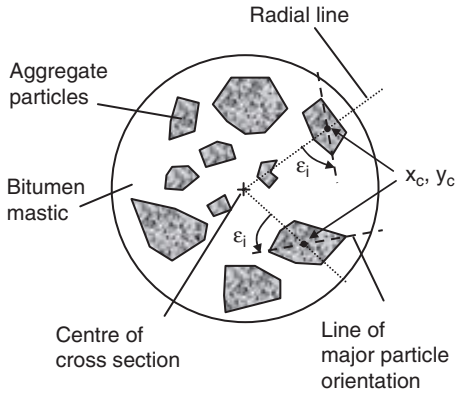

Figure 4. Schematic diagram indicating aggregate orientation relative to centre of core.

Aggregate orientation

Each mode of compaction has its own specific type of loading and boundary conditions which inevitably have an effect on the resulting aggregate orientation in the compacted asphalt mixture. When studying aggregate orientation, a point of reference from which measurements should be made needs to be defined. If radial or circumferential particle alignment is to be investigated it needs to be considered relative to the core centre, as opposed to an imposed arbitrary $x-y$ axes. Figure 4 is a schematic diagram representing the horizontal plane of an asphalt specimen, indicating the particle orientation ε_i. The particle orientation ε_i is defined as the angle between the radial line (connecting the centre of the core to the centre of the particle) and the line of major particle orientation. It is calculated from the knowledge of the particle co-ordinates, centre of the specimen co-ordinates and the vertical particle angle β. The angle ε_i varies from 0° to 90°, i.e. it is always the minor angle between the

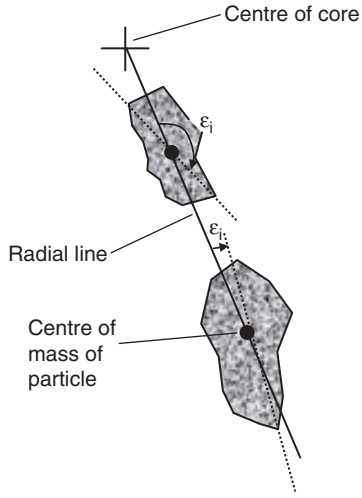

Figure 5. Particles aligned in radial directions.

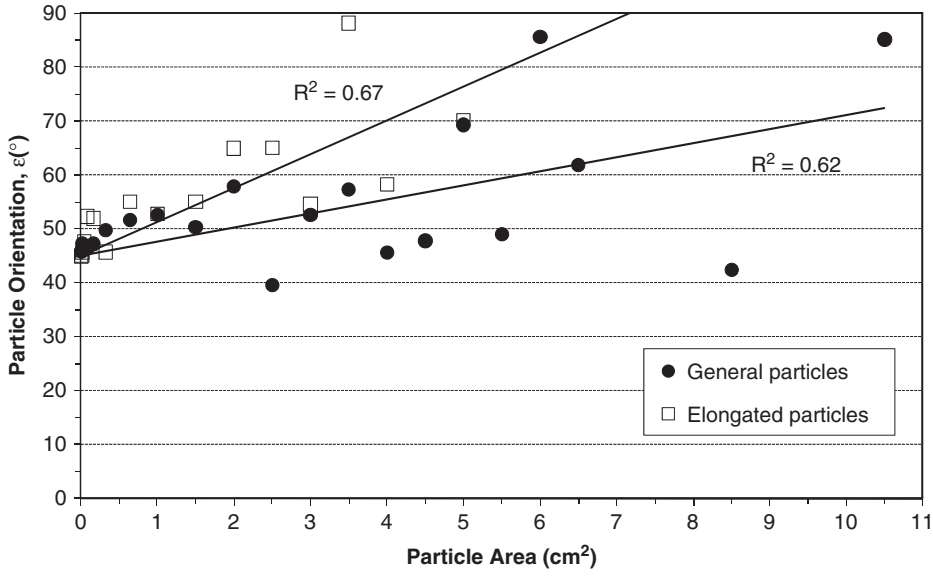

Figure 6. Plot of particle orientation versus particle size for a gyratory-compacted specimen.

radial line and the line of major orientation. If $\varepsilon_i = 0°$, then the particles are aligned in a radial direction, and if $\varepsilon_i = 90°$, then the particles are aligned in a circumferential direction, i.e. parallel to the circumference. It is worth noting that if the particles have a random distribution then the average value of ε_i will be 45°. Calculating the angle ε_i in this way ensures against the scenario depicted in Figure 5, where two particles are aligned in very similar directions but have widely varying angles of ε_i. In this scenario, any averaging of angles would yield meaningless results.

The behaviour of the aggregate particles was investigated as a function of their size, shape and depth in the sample. There is a relatively large spread of aggregate sizes within a typical asphalt mixture, spanning from dust to particles with a nominal diameter of 28 mm for the asphalt mixtures included in this study. The particles were split by their particle area range with an average (weighted) circumferential particle orientation being calculated for each particle area range according to Equation 5.

$$\varepsilon_w = \frac{\sum_{i=1}^{i=n} \varepsilon_i a_1}{\sum_{i=1}^{i=n} a_i}, \quad (5)$$

where ε_w is the weighted circumferential angle for a particle area range, n is the total number of particles within the particle area range, ε_i is the individual particle orientation relative to the centre and a_i is the individual particle area (Hunter *et al.* 2004a). The weighted circumferential angles (ε_w) for the various particle area ranges were obtained for the four surfaces (Figure 2) of each core and subsequently averaged for the 30 specimens of each compaction method. The analysis was also undertaken on 'elongated' particles to investigate whether they were subject to a greater degree of re-orientation. In this study, an elongated particle is classed as having an aspect (length/width) ratio of greater than two.

A particle orientation plot is shown in Figure 6 for the gyratory-compacted 28-mm DBM asphalt mixture for all particles as well as elongated particles. With both gyratory and vibratory samples there is a general increase in particle orientation tending towards 90° with increasing particle area with this trend being more pronounced for elongated particles. The variance in the results from the lines of best fit shown in Figure 6 is indicative of the results for gyratory- and vibratory-compacted specimens, i.e. there is a general trend towards circumferential particle orientation with increasing particle size, but there are plenty of exceptions to the rule. The gradient of the line of best fit in Figure 6 has units of degrees per cm^2 VSA (particle area) with the zero particle size (y intercept) being fixed at 45°. The gradients for three of the asphalt mixture types and the four compaction methods (three laboratory and field compaction) have been used to determine the aggregate orientation at increasing particle sizes in Tables 2–4.

Table 2. Aggregate orientation of different sizes for 28-mm DBM material.

Particle size (cm^2)	Aggregate orientation (°)			
	Gyratory	Slab	Vibratory	Field
0	45.0	45.0	45.0	45.0
2	48.1	46.5	49.9	45.7
4	51.2	47.9	54.8	46.5
6	54.4	49.4	59.7	47.2
8	57.5	50.8	64.6	48.0
10	60.6	52.3	69.5	48.7

Table 3. Aggregate orientation of different sizes for 20-mm HMB material.

	Aggregate orientation (°)			
Particle size (cm^2)	Gyratory	Slab	Vibratory	Field
0	45.0	45.0	45.0	45.0
2	47.5	46.0	48.0	45.6
4	49.9	47.1	51.0	46.3
6	52.4	48.1	54.1	46.9
8	54.8	49.2	57.1	47.5

Table 4. Aggregate orientation of different sizes for 14-mm surfacing.

	Aggregate orientation (°)	
Particle size (cm^2)	Vibratory	Field
0	45.0	45.0
2	43.9	45.7
4	42.8	46.3
6	41.7	47.0

The results indicate that circumferential alignment of aggregate particles occurs more in gyratory- and vibratory-compacted specimens than in slab- or field-compacted specimens. In addition, this behaviour is more pronounced for larger aggregate size mixtures (28-mm DBM and 20-mm HMB) than the smaller size 14 mm surfacing, where the vibratory-compacted specimens actually show a slight radial alignment. In general, there is a better agreement between slab- and field-compacted aggregate alignment (orientation) than between the two mould-based techniques (gyratory and vibratory) and field compaction. Both the slab- and field-compacted specimens display a more random particle orientation, than the circumferential aggregate orientation found for gyratory and vibratory compaction as highlighted in Figure 7.

The reason for the circumferential orientation is difficult to verify, but two likely contenders are (i) boundary effects due to the confining nature of the gyratory and vibratory moulds and (ii) the circumferential shear stress imparted by the inclined plate of the gyratory compactor and the kneading action of the vibratory hammer. The relative influence of these two effects can be investigated by removing the influence of the mould boundary by altering the compaction and testing methodology as shown in Figure 8. After gyratory compaction and extraction, a set of asphalt mixture specimens were trimmed to produce 150 mm diameter by 60 mm high specimens for subsequent image analysis, density and mechanical property testing. The top and bottom 20 mm of the compacted specimens (high air void content sections) were removed in order to obtain as consistent a void content distribution as possible as described by Masad *et al.* (1999, 2002). The 150 mm diameter specimens were then cored to obtain 100 mm diameter by 60 mm high specimens as shown in Figure 9.

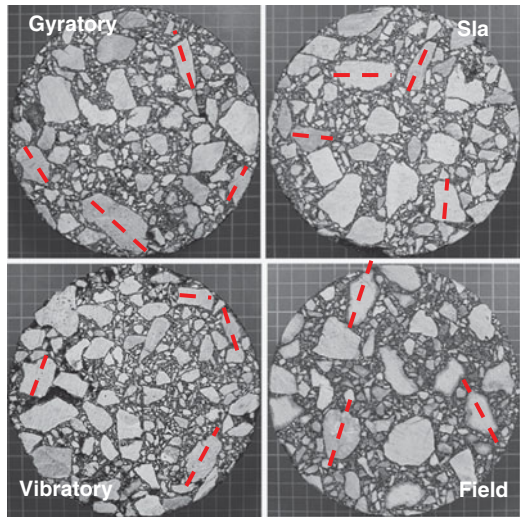

Figure 7. Horizontal sections through 150-mm diameter cores of 28-mm DBM.

The aggregate orientation as a function on increasing particle size (area) for the different sized specimens is presented in Table 5. However, instead of seeing a reduction in slope (circumferential particle orientation) and a more random distribution of aggregate orientations, the 100-mm specimens had very similar orientations (for both the gyratory and vibratory specimens). The results in Tables 2–4 show that slab-compacted specimens exhibited a smaller degree of circumferential alignment compared to gyratory and vibratory compaction, with this reduced orientation thought to be due to the lack of mould confinement as the specimens were cored from a larger slab. However, there was still a degree of circumferential orientation that was thought to be due to the coring process producing erroneous elongated particles that were analysed as circumferentially orientated particles. A similar process was thought to be happening with the cores from the 150-mm diameter gyratory and vibratory specimens as shown in Figure 10.

To overcome this possible error, the 150-mm diameter images were reanalysed by using the computer software to artificially core the larger specimen by only determining the orientation of those particles that had their centres within a radius of 50 mm from the centre of the specimen as shown in Figure 11.

The results in Table 5 clearly show that using this approach leads to a large reduction in the particle orientation and, therefore, a more random particle orientation for both the gyratory- and vibratory-compacted specimens. The values shown in Table 5 for the computer-trimmed 100-mm cores are similar to the values obtained for slab-compacted specimens (Hunter *et al.* 2004a, Iwama *et al.* 2007).

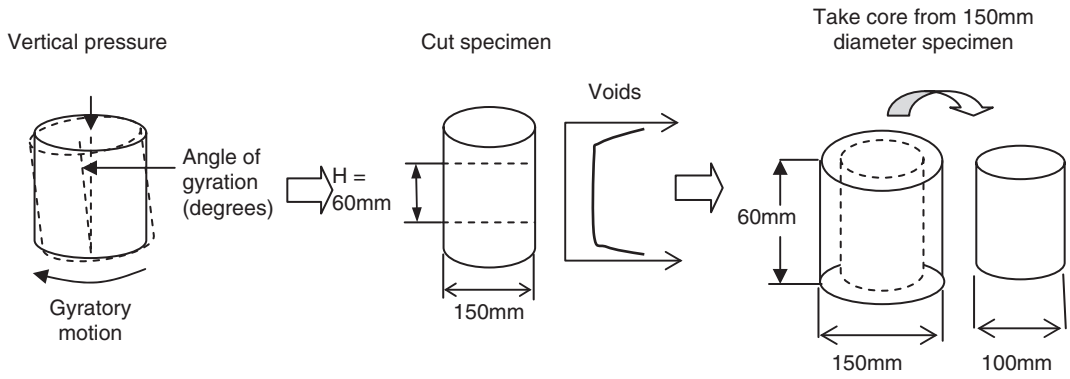

Figure 8. Specimen dimensional testing methodology for gyratory compaction.

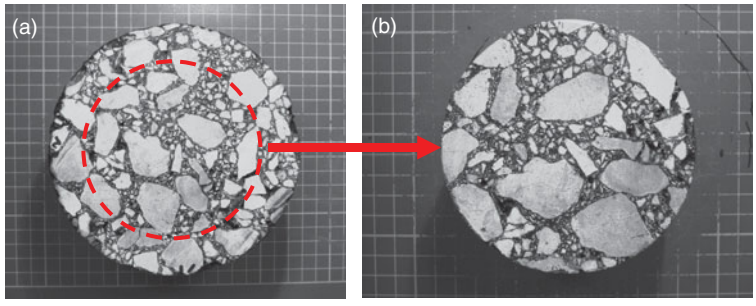

Figure 9. Coring process on gyratory and vibratory cores (a) 150-mm diameter, (b) 100-mm diameter.

Aggregate segregation

Aggregate segregation is another parameter by which the aggregate matrix may be described. Ideally, a specimen made up of a continuously graded mixture should have an even distribution of particles across its volume. However, due to inevitable segregation which occurs during all compaction processes, this is rarely the case. In this study, the aggregate segregation has been considered from two perspectives: (i) relative to the centre of the cross-section using sectors (radial segregation) and (ii) by considering the inner and outer regions of the specimen cross-section (regional segregation) (Hunter *et al.* 2004a).

For the radial segregation, the method of analysis involved splitting the cross-section into sectors of 5°, with the entire cross-section comprising 72 sectors. If the aggregate particles in 18 adjacent sectors are summed up then the area of aggregate present in a quarter of the cross-section is obtained. By shifting around the cross-section by 5° the area of aggregate in 72 different quarters can be calculated, from which the maximum may be selected. This process is shown graphically in Figure 12 where the individual sectors have been denoted by α. This process enables the quarter with the maximum aggregate density to be located as well as the aggregate densities in the

Table 5. Aggregate orientation of 150-mm and 100-mm diameter specimens for 28-mm DBM material.

	Aggregate orientation (°)					
	Gyratory			Vibratory		
Particle size (cm^2)	150 mm	100 mm	C100 mm	150 mm	100 mm	C100 mm
0	45.0	45.0	45.0	45.0	45.0	45.0
2	48.1	48.1	45.3	49.9	49.5	45.8
4	51.2	51.1	45.7	54.8	54.0	46.6
6	54.4	54.2	46.0	59.7	58.6	47.3
8	57.5	57.2	46.4	64.6	63.1	48.1
10	60.6	60.3	46.7	69.5	67.6	48.9

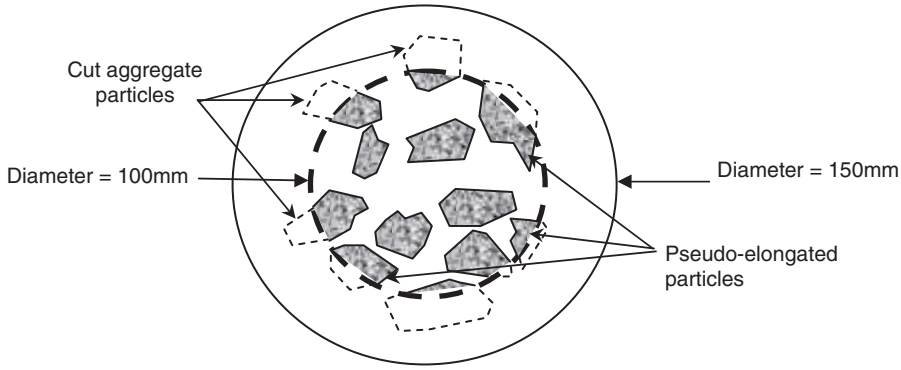

Figure 10. Schematic representation of bisected aggregate particles.

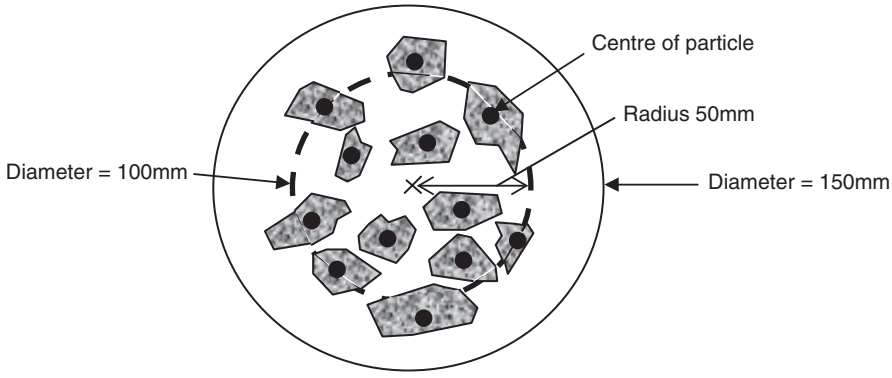

Figure 11. Schematic representation of computer-trimmed 100-mm diameter specimen.

remaining three quarters. An evenly distributed asphalt specimen should have relatively close cumulative aggregate area values across all four quarters for all particle sizes.

The segregation ratio (maximum divided by minimum quarter) for the 28-mm DBM, 20-mm HMB and 14-mm surfacing as a function of compaction method are shown in Figure 13. The ratios indicate that slab-compacted specimens have less radial segregation than gyratory and vibratory specimens. However, the results also show that field-compacted specimens generally tend to have a relatively high degree of radial segregation particularly for larger aggregate size mixtures. Overall, the coarser mixtures (28-mm DBM and 20-mm HMB) tend to have higher degrees of radial segregation than the finer mixtures (14 mm surfacing).

For the regional segregation, the cross-section of the cores was split into inner and outer regions of equal area and the average VSA in the respective regions calculated.

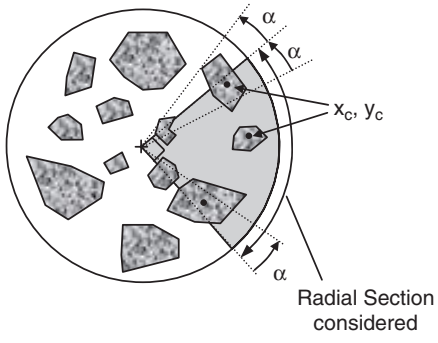

Figure 12. Schematic diagram indicating calculation of radial segregation.

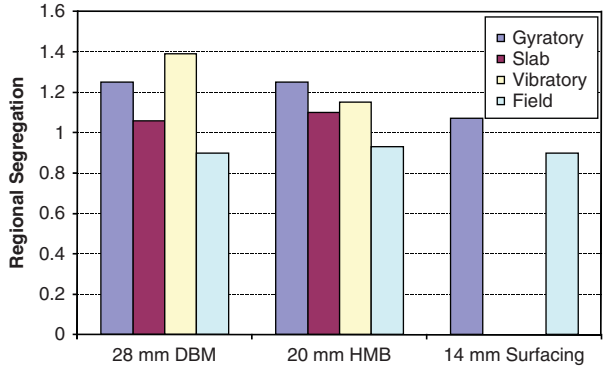

Figure 13. Particle radial segregation as a function of compaction method.

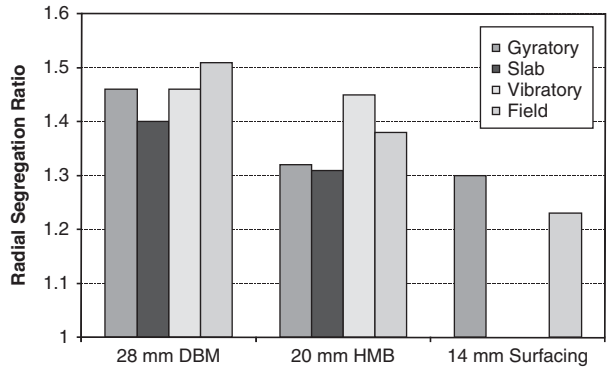

Figure 14. Particle regional segregation as a function of compaction method.

The ratio of inner to outer VSA is presented in Figure 14 and shows that a relatively large difference in average VSA exists for the vibratory- and gyratory-compacted samples, possibly due to the vibration and gyratory action causing larger particles to migrate to the boundary of the sample. This behaviour is consistent with the findings of Tashman *et al.* (2001). The slab-compacted samples showed a near uniform particle size distribution across the regions considered, while field cores showed a slightly higher concentration of aggregate in the inner region.

Mechanical property results

Asphalt mixture stiffness

The main objective of the testing programme was to establish which mechanical parameters were most sensitive to the mode of compaction. The volumetric proportions (air void contents) together with the stiffness results from the ITSM are presented in Tables 6–9 for the 28-mm DBM, 20-mm HMB, 14-mm surfacing and 32-mm HMB asphalt materials. The average, standard deviation and coefficient of variation were recorded for the different compaction methods. In general, the results of the air voids and stiffness moduli for the 28-mm DBM asphalt mixture are relatively consistent with low coefficients of variation within the range of 8–15% for the air voids and 7–14% for stiffness modulus for the laboratory compaction methods. The coefficients of variation for the 20-mm DBM, 14-mm surfacing and 32-mm HMB asphalt mixtures are slightly higher with the field variations tending to be higher for all four mixtures. The increased variability associated with the air void contents of the laboratory-compacted 20-mm, 14-mm and 32-mm asphalt mixture specimens may be partly due to the use of stiffer and polymer-modified bitumens in these materials compared to the 28-mm DBM mixture (Hunter *et al.* 2009).

The mean stiffness moduli as a function of mean air voids for the 14-mm asphalt mixture are plotted in Figure 15. In this plot, the vibratory- and field-compacted specimens are of comparable stiffness if the difference in air void content is accounted for (increased air voids for field cores). The gyratory-compacted specimens, with similar air void content to the site-compacted specimens, have almost double the mean stiffness modulus. The combined results for all four asphalt mixture types (Table 6–9) show a degree of scatter with no one laboratory compaction method consistently producing either extremely high or low stiffness modulus specimens. However, in general the mould-based compaction methods (gyratory and vibratory) tend to produce specimens of

Table 6. Volumetric and stiffness modulus results for 28-mm DBM asphalt mixture.

	Compaction method			
Properties	Gyratory	Slab	Vibratory	Field
Average air voids (%)	3.1	3.0	2.8	8.2
Standard deviation air voids (%)	0.4	0.4	0.2	1.8
CoV air voids (%)	13	14	8	22
Average stiffness (MPa)	7906	7323	10,089	1891
Standard deviation stiffness (MPa)	596	540	932	269
CoV stiffness (%)	8	7	9	14

Table 7. Volumetric and stiffness modulus results for 20-mm HMB asphalt mixture.

	Compaction method			
Properties	Gyratory	Slab	Vibratory	Field
Average air voids (%)	4.0	2.7	2.9	1.6
Standard deviation air voids (%)	1.6	0.9	0.9	0.7
CoV air voids (%)	40	33	32	42
Average stiffness (MPa)	10,601	8173	10,022	5476
Standard deviation stiffness (MPa)	882	493	2066	586
CoV stiffness (%)	8	6	21	11

Table 8. Volumetric and stiffness modulus results for 14-mm surfacing material.

	Compaction method		
Properties	Gyratory	Vibratory	Field
Average air voids (%)	3.4	2.2	2.8
Standard deviation air voids (%)	0.6	0.7	0.6
CoV air voids (%)	19	31	20
Average stiffness (MPa)	2889	2104	1565
Standard deviation stiffness (MPa)	228	252	196
CoV stiffness (%)	8	12	13

Table 9. Volumetric and stiffness modulus results for 32-mm HMB asphalt mixture.

Properties	Compaction method			
	Gyratory	Slab	Vibratory	Field
Average air voids (%)	3.8	3.4	4.4	4.1
Standard deviation air voids (%)	1.3	0.5	0.5	1.7
CoV air voids (%)	34	15	6	42
Average stiffness (MPa)	11,003	10,327	12,233	6411
Standard deviation stiffness (MPa)	2050	841	675	859
CoV stiffness (%)	19	8	6	13

higher stiffness than the roller- (slab) and field-compacted specimens as shown in Figure 16 where the average stiffness values, relative to gyratory compaction, are depicted.

Assuming that the mixture design, mixing procedures, compaction temperatures and volumetrics are identical, the reasons for the different stiffness results can be linked to the internal structure of the asphalt mixture matrix. The results in this and other studies have established that a circumferential aggregate orientation occurs in mould-based compaction (Hunter *et al.* 2004a), as well as a distribution of aggregate sizes between the inside and outside of the specimen (Masad *et al.* 1999, 2002, Tashman *et al.* 2001, 2002). These studies have also revealed a 'bath tub' air void distribution in gyratory-compacted specimens, i.e. far higher air void content at the surfaces in contact with the loading platens. In contrast, linear kneading (vibratory) compactors produce a near linear increase of air void content with depth. These distinct particle arrangements within a specimen will have a direct influence on the micro-mechanical properties as manifested through variations in stiffness modulus between compaction methods.

The aggregate orientations shown in Table 5 indicate that a more random particle orientation (aggregate matrix)

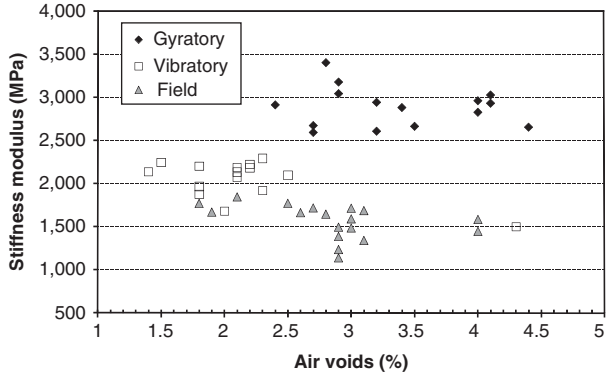

Figure 15. Stiffness modulus against air voids for different compaction modes – 14-mm surfacing asphalt mixture.

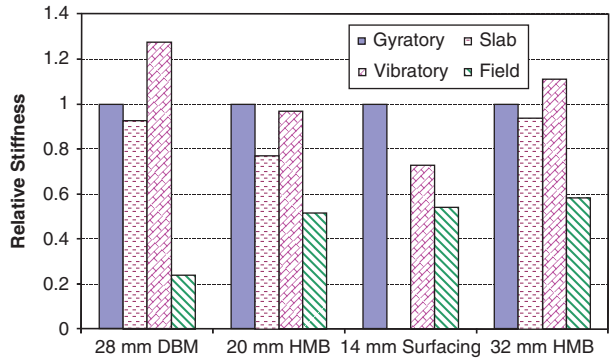

Figure 16. Asphalt mixture stiffness relative to gyratory-compacted asphalt stiffness.

can be produced for mould-based compaction methods by coring 100-mm diameter specimens from larger 150-mm diameter specimen. Although, this has only had a marginal effect on stiffness modulus as shown in Table 10, it is interesting to note that both the stiffness and air void contents of the smaller specimens are lower than those of the larger specimens and, therefore, closer to the slab and field values.

Asphalt mixture rutting resistance

The permanent deformation results obtained from the RLAT for the 20-mm asphalt mixture are shown in Figure 17 as a function of air void content. The results, if viewed as a whole, show an increase in resistance to permanent deformation of the specimens with an increase in air voids, levelling out at approximately 3.5% air void content. Gibb (1996) reported a similar relationship is his study where poor resistance to permanent deformation was observed in both vibratory-compacted specimens and field cores with low air voids, typically below 3% for a range of UK asphalt mixtures. He hypothesised that this was due to insufficient void space to accommodate the bitumen/fines mortar, resulting in loss of frictional contact between aggregate particles under loading. Furthermore, data

Table 10. Volumetric and stiffness results for the 150-mm and 100-mm diameter 28-mm DBM asphalt specimens.

Properties	Gyratory		Vibratory	
	150 mm	100 mm	150 mm	100 mm
Average air voids (%)	2.8	2.5	3.1	2.7
Standard deviation air voids (%)	0.8	1.1	1.2	1.0
CoV air voids (%)	28	42	37	37
Average stiffness (MPa)	6786	6304	8042	7435
Standard deviation stiffness (MPa)	566	597	670	642
CoV stiffness (%)	8	9	8	9

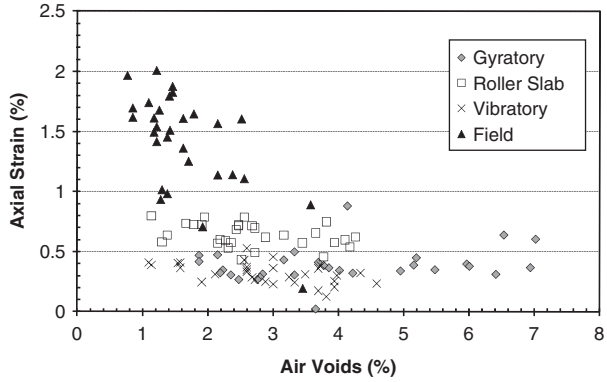

Figure 17. Permanent strain versus air voids for different compaction modes – 20-mm DBM asphalt mixture.

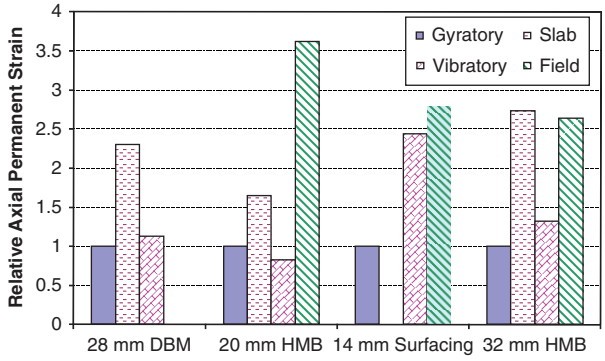

Figure 18. Asphalt mixture permanent strain relative to gyratory-compacted permanent strain.

relating to continuously graded DBM materials indicated an 'optimum void content range' typically 3–8% within which the asphalt mixture performance remained relatively constant. Above 8–10% air void content, there is a marked reduction in resistance to permanent deformation. Another interesting observation from this study was that at high air voids (>10%) there is little difference in permanent deformation performance between laboratory- and field-compacted specimens indicating that the degree of compaction is more significant than the method of compaction (Gibb 1996).

Looking at the different compaction methods, the field specimens are considerably different from the laboratory-compacted specimens both in terms of axial strain (mean axial strain of 1.41%) and air voids (mean air voids of 1.7%). The slab-compacted specimens have a higher air void content (2.7%) and significantly lower axial strain (0.64%). There is a further increase in resistance to permanent deformation for the gyratory- (average permanent strain of 0.40%) and vibratory- (average permanent strain of 0.32%) compacted specimens. It should be noted that the gyratory-compacted specimens have higher mean air void content (4.0%) than the roller- and vibratory-compacted specimens (2.7% and 2.9% respectively). In general, the data suggest that mould-based compaction methods (gyratory and vibratory) produce specimens with greater resistance to permanent deformation compared to roller compaction. This can be clearly seen over the air void range of 2–4% for the gyratory-, vibratory- and roller-compacted asphalt mixtures specimens in Figure 17.

The permanent deformation performance of all the asphalt mixtures, quantified by the ultimate percentage strain after 3600 cycles, is presented in Table 11, with the permanent deformation performance relative to gyratory compacted specimens shown in Figure 18. The results clearly show the superior permanent deformation performance of the gyratory- and vibratory-compacted specimens compared to the slab and particularly the field compacted cores. Although the permanent strain results for the slab and field specimens of the 32-mm HMB are almost identical, the strains for the field specimens are more than double that of the slab cores for the 20-mm HMB mixture.

Table 11. Average permanent strain results from RLAT.

	Permanent strain (%) after 3600 loading cycles			
Asphalt mixture	Gyratory	Slab	Vibratory	Field
28-mm DBM mixture	0.58	1.33	0.65	–
20-mm DBM mixture	0.39	0.64	0.32	1.41
14-mm surfacing	0.56	–	1.36	1.56
32-mm DBM mixture	0.51	1.39	0.67	1.34

Asphalt mixture fatigue

The fatigue results from the ITFT for the 28-mm DBM asphalt mixture are shown in Figure 19 in the form of the fatigue relationship defined in Equation 4 and using a strain criterion. The seven sets of fatigue data, representing the three compaction methods (gyratory, vibratory and roller slab) and five laboratories (all gyratory compaction), all lie on the same fatigue function (Hunter *et al.* 2009). It is arguable whether any significantly different fatigue lines exist between the data-sets beyond the natural variation associated with a fatigue (failure) test. This is substantiated by an R^2 value of 0.85 for the fatigue line of best fit for the aggregated data-sets.

Conclusions and discussion

The mechanical property results show that in general mould-based compaction methods (gyratory and vibratory) form asphalt mixture specimens of greater stiffness and resistance to permanent deformation. Site cores appear to lie at the other end of the spectrum in terms of

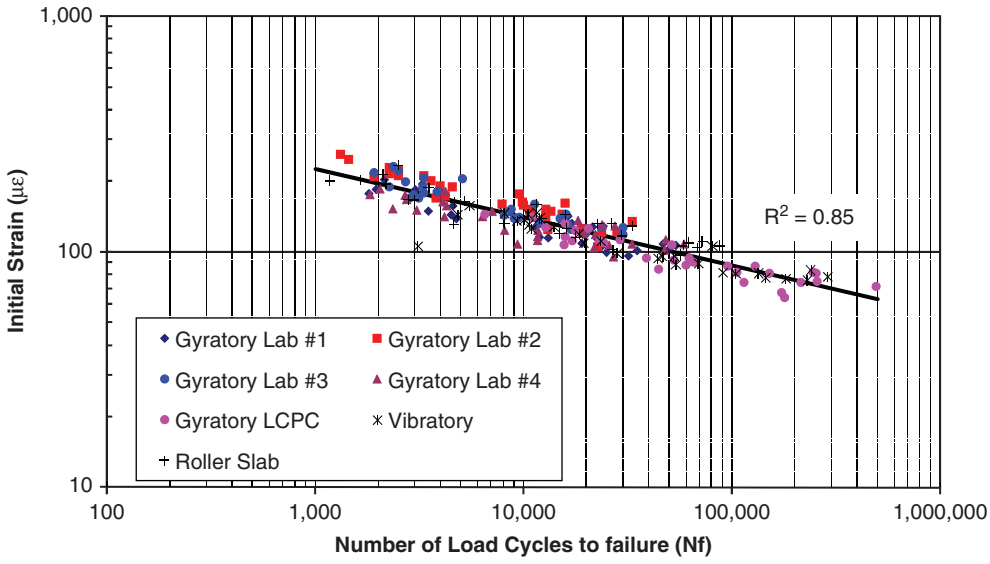

Figure 19. Fatigue as a function of laboratory compaction method for 28-mm DBM.

mechanical performance and, in general, have lower stiffness and increased susceptibility to permanent deformation. Conversely, the mode of compaction does not appear to influence the fatigue response of an asphalt mixture (unique fatigue relationship for each asphalt mixture independent of compaction method). However, there are several exceptions to these general trends which may be seen from the data presented in this article. Indeed within a given compaction method there will be considerable scope for variation, as demonstrated by the difference in stiffness between the type of gyratory compactor (28-mm asphalt mixture) and operation of roller compactors (20-mm asphalt mixture) (Hunter *et al.* 2009). Sousa *et al.* (1991) also recognised that compactors within a given mode of compaction may manufacture specimens with quite different properties. They used the example of a kneading compactor, stating that the compaction parameters (size of foot, number of tamps, size of specimen, thickness of layer, tamping pressure) and the variation of these parameters will almost certainly affect many mixture properties linked to asphalt performance. This view was further reinforced by the findings of Harvey *et al.* (1994).

Within any one generic compaction mode there would appear to be compaction variables which have an effect on the stiffness and permanent deformation of the specimens for a given air void content. For example, in gyratory compaction it could be the angle of gyration or the compaction pressure. For roller (slab) compaction probable parameters are compaction pressure and roller speed. In addition, the importance of sample preparation, bitumen and aggregate heating temperatures and duration and finally mixing procedures cannot be overlooked. All these parameters undoubtedly have an influence on the micro-mechanical behaviour of the coated aggregate particles.

Based on the findings from this study on the comparison between laboratory and field compaction in terms of the physical particle arrangement and mechanical properties of asphalt mixtures, the following conclusions are relevant:

Gyratory and vibratory compactions produce asphalt mixture specimens that are susceptible to circumferential particle orientation with the degree of circumferential orientation increasing with particle size. This aggregate orientation is probably due to boundary conditions associated with the moulds used with these compaction methods.

The circumferential particle alignment associated with gyratory and vibratory compaction can be eliminated to a certain degree by removing smaller diameter specimens for testing from larger diameter compacted specimens. This has the effect of producing an internal aggregate structure similar to that found in field- and slab-compacted specimens.

In terms of radial and regional segregation, the three laboratory compaction methods and field compaction showed various degrees of particle segregation. The gyratory and vibratory specimens showed a higher radial segregation ratio than slab-compacted specimens but not as high as field cores. Regional segregation tended to be more prevalent in vibratory- and gyratory-compacted specimens compared to slab- and field-compacted specimens.

Overall, slab-compacted specimens tend to show closer correlation with field cores than gyratory- and vibratory-compacted specimens.

The results show that mould-based compaction methods (gyratory and vibratory) generally produce stiffer specimens with higher resistance to permanent deformation when compared to slab 'roller'-compacted specimens and field compacted cores of comparable air voids. This may be a result of possibly higher compaction energies being associated with the gyratory and vibratory compaction methods.

References

Airey, G.D., Hunter, A.E., Collop, A.C., and Zoorob, S.E., 2006. Comparison of field and laboratory compacted asphalt mixtures. *In: 10th international conference on asphalt pavements*, Quebec City. Leiden, The Netherlands: Balkema, Vol. 1, 35–46.

Brown, S.F. and Gibb, J.M., 1996. Validation experiments for permanent deformation testing of bituminous mixtures. *Journal of the Association of Asphalt Paving Technologists*, 65, 255–299.

Brown, S.F. and Gibb, J.M., 1999. Effects of compaction on mechanical properties of asphalt mixtures. *In: 7th conference on asphalt pavements for southern Africa*, Victoria Falls, Zimbabwe. Cape Town: CAPSA.

Consuegra, A., Little, D.N., Quintas, H.V., and Burati, J., 1989. Comparative evaluation of laboratory compaction devices based on their ability to produce mixtures with engineering properties similar to those produced in the field. *Transportation Research Record*, 1228, 80–87.

Gibb, J.M., 1996. Evaluation of resistance to permanent deformation in the design of bituminous paving mixtures. Thesis (PhD), University of Nottingham.

Harvey, J. and Monismith, C.L., 1993. Effects of laboratory asphalt concrete specimen preparation variables on fatigue and permanent deformation test results using strategic highway research programme A-003A proposed testing equipment. *In*: *Transportation Research Record 1417*. Washington, DC: Transportation Research Board, 38–48.

Harvey, J., Monismith, C.L., and Sousa, J.B., 1994. An investigation of field and laboratory compacted asphalt-rubber, SMA, recycled and conventional asphalt-concrete mixes using SHRP Project A-003A equipment. *Journal of the Association of Asphalt Paving Technologists*, 63, 511–560.

Hunter, A.E., Airey, G.D., and Collop, A.C., 2004a. Aggregate orientation and segregation in laboratory compacted asphalt samples. *Transportation Research Record*, 1891, 8–15.

Hunter, A.E., Airey, G.D., and Collop, A.C., 2004b. Influence of compaction method on asphalt mixture internal structure and mechanical properties. *In: 3rd eurasphalt and eurobitume congress*, Vienna, Vol. 2, 1868–1877.

Hunter, A.E., McGreavy, L., and Airey, G.D., 2009. Effect of compaction mode on the mechanical performance and variability of asphalt mixtures. *ASCE Journal of Transportation Engineering*, 135 (11), 839–851.

Iwama, M., Airey, G.D., and Hunter, A.E., 2007. Influence of asphalt mixture compaction method and specimen size on internal structure and mechanical properties. *In: International conference on advanced characterisation of pavement and soil engineering materials*, Athens. Leiden, The Netherlands: Taylor & Francis, Vol. 2, 1063–1073.

Masad, E. and Button, J., 2004. Implications of experimental measurements and analyses of the internal structure of HMA. *In: Proceedings of the 83rd TRB annual meeting*. Washington, DC: Transportation Research Board.

Masad, E., Jandhyala, V.K., Dasgupta, N., Somadevan, N., and Shashidhar, N., 2002. Characterization of air void distribution in asphalt mixes using X-ray computer tomography. *Journal of Materials in Civil Engineering*, 14, 122–129.

Masad, E., Muhunthan, B., Shashidhar, N., and Harman, T., 1999. Quantifying laboratory compaction effects on the internal structure of asphalt concrete. *Transportation Research Record*, 1681, 179–185.

Nevitt, H.G., 1959. Some sources of stability measurement variations. *Association of Asphalt Paving Technologists*, 28, 16–34.

Renken, P., 2000. Influence of specimen preparation onto the mechanical behaviour of asphalt mixtures. *In: 2nd eurasphalt & eurobitume congress,* Barcelona. Breukelen, The Netherlands: Foundation Eurasphalt, 729–735.

Shashidar, N., 1999. X-Ray tomograpy of asphalt concrete. *Transportation Research Board*, 1681, 186–192.

Sousa, J.B., Deacon, J.A., and Monismith, C.L., 1991. Effect of laboratory compaction on permanent deformation characteristics of asphalt-aggregate mixtures. *Journal of the Association of Asphalt Paving Technologists*, 60, 533–585.

Tashman, L., Masad, E., Peterson, B., and Saleh, H., 2001. Internal structure analysis of asphalt mixes to improve the simulation of superpave gyratory compaction to field conditions. *Journal of the Association of Asphalt Paving Technologists*, 70, 605–645.

Tashman, L., Masad, E., D'Angelo, J., Bukowski, J., and Harman, T., 2002. X-Ray tomography to characterize air void distribution in superpave gyratory compacted specimens. *The International Journal of Pavement Engineering*, 3 (1), 19–28.

Vallerga, B., 1951. Recent laboratory compaction studies of bituminous paving mixtures. *Association of Asphalt Paving Technologists*, 20, 117–153.

Von Quintas, H.L., Scherocman, J.A., Hughes, C.S., and Kennedy, T.W., 1991. *Asphalt-aggregate mixture analysis system, AAMAS*. National Cooperative Highway Research Program Report 338. Washington, DC: Transportation Research Board.

Yue, Q.Z., Bekking, W., and Morin, I., 1995. Application of Digital Image Processing to Quantitative Study of Asphalt Concrete Microstructure. *Transportation Research Record*, 1492, 53–60.